CO_2-Brine Relative Permeability Measurements at Reservoir Conditions: how to reconciliate SS and USS methods?

Matthieu Mascle[1], Ameline Oisel[1], Per Kristian Munkerud[2], Einar Ebeltoft[3], Olivier Lopez[2], Colin Pryme[2], Souhail Youssef[1]*

[1]IFP Energies Nouvelles, 1 et 4 avenue de Bois-Préau, 92852 Rueil-Malmaison, France
[2]Equinor ASA, Trondheim, Norway
[3]Equinor ASA, Bergen, Norway

Abstract. Injection of CO_2 into deep saline aquifers for geological carbon sequestration is being developed worldwide as a large-scale technology to reduce the greenhouse effect. Successful management of such industrial-scale projects requires accurate characterization of reservoir dynamic properties. However, literature review shows a lack of CO_2-brine relative permeability measurements under reservoir conditions for most storage cases, as well as a non-consensus on the measurement methods that partially explain the discrepancies observed in published results. The objectives of the work presented here is to reconciliate these methods and to get "best practices" when measuring kr-curves with CO_2. CO_2/brine kr-curves have been measured using two protocols (steady-state and unsteady-state methods), on a homogenous Grès-de-Fontainebleau sandstone. Experiments were conducted at reservoir conditions (54°C, 90bars), using the mini-coreflood injection platform CAL-X™. This set-up limits the plug size to a typical core length of 20mm but provides a quantitative access to the local saturations. We found that the combination of the different methods allows to derive the most reliable curves. As experiments on small samples are an order of magnitude faster than measured on standard sample, the combination of these methods is made possible in a reasonable time (few days). Finally, using 2D radiography to monitor local saturation has demonstrated to be a key element for the Kr/Pc curves interpretations. It provides the possibility to quality check the displacement homogeneity, in both radial and vertical directions.

1 Introduction

According to a recent report from the Intergovernmental Panel on Climate Change (IPCC), the objective of limiting the global warming to +1.5°C can only be reached by removing tens of giga-tons of CO_2 per year ($GtCO_2$/yr) from the atmosphere [1]. Many publications [2–4] review the different technologies that need to be used to address this objective. Among them, the sequestration of CO_2 into subsurface geological formations is the most mature technique, accounting today for roughly 4 mega-tons of CO_2 per year ($MtCO_2$/yr) [2] (not accounting for CO2 EOR projects).

When injected into deep saline aquifers, the primary trapping mechanism for CO_2 is the geology structure and stratigraphy. The CO_2 migration to the surface is prevented by a reservoir seal: a geological formation characterized by a high capillary pressure and a low permeability. The secondary trapping mechanisms involve the capillary trapping of CO_2 in the porous reservoir and its solubilization in the brine aquifer [5]. Both these trapping mechanisms involves the understanding of the multi-phases flow of CO_2 and brine through the porous media. These flow properties (namely capillary pressure P_c and relative permeabilities curves k_r-curves) control the spread of the CO_2 plumes through the reservoir and its boundaries [6–9]. Those properties also directly give the quantity of CO_2 that remains trapped by capillary forces after an imbibition cycle [8, 10–12] (referred here as the residual gas saturation S_{rg}). Their importance has also been pointed-out by [13] when estimating the wells' injectivity or when sizing the surface facilities. To wrap it up, the short- and long-term viability of CO_2 underground storage projects (CUS) largely depends on these flow properties.

Yet, a review from the Global CCS Institute and Stanford University [14] pointed out the great variability of k_r-curves data available in the literature for the CO_2/brine pair of fluids. According to their paper, this variability is not explained by differences in the experimental conditions for the different studies used, but mainly by the methodology and the protocols applied when running the experiments in the laboratory. Two methods have been largely used to measure k_r-curves: the steady-state method (SS) and the unsteady-state method

* Corresponding author: matthieu.mascle@ifpen.fr

(US). The first one involves co-injecting the two fluids at varying fractional flowrate (f_w), while the second one relies on a monophasic injection but requires history match for interpretation with consideration of capillary end effects (CEE). The semi-dynamic method (SDM), initially designed to measure P_c curves [15] can also be used to estimate the k_r-curves with additional analytical interpretations [16, 17].

The question of whether the k_r-curves should be measured using the SS- or the US-method is an old debate. The SS-method has often been considered as the most reliable method for k_r-curves measurement [18], as it favors homogenous saturations through the core, especially when advert fluids mobility ratios are involved [18, 19]. The SS-method limits the dependency of the measurement to the injection total flowrate [20] and the experimental points measured at each f_w (with an exception for the monophasic injections: f_w=1 and f_w=0) are easily interpreted using an analytical solution derived from the simplified Darcy's equations (assuming constant P_c). The reason behind these advantages is the mitigation of the CEE when using fluids co-injections [18, 21]. CEE is the major drawback of the US-method, leading to an accumulation of the wetting phase near the core outlet due to capillary pressure boundary conditions [22–24]. This accumulation causes both an underestimation of the non-wetting fluid saturation and of the k_r-values (in the sense of lower k_r-values estimated). Yet, this method is often preferred in the industry as it provides quicker results and requires less quantities of fluids. CEE is generally dampened in laboratory by using higher fluids viscosities, high flowrates [25, 26], or longer cores [27, 28]. But these solutions are not always feasible or are no longer representative of the reservoir conditions.

Another advantage of the SS-method over the US-method is the estimation of the k_r-values for low and intermediates non-wetting phase saturations [29]. During a monophasic non-wetting phase injection (US-method), the average phase saturation is progressively increased from 0% to higher values. However, the low and intermediate saturations are not represented at local scale, as the non-wetting phase propagates with a front [24]. This limits the possibility to accurately constrain the k_r-curves estimation for these saturations, even when using history match techniques.

Finally, the irreducible water saturation (often referred as the S_{wir} value) remains difficult to reach with both these methods (SS and US) [30, 31], while it is a key input for CO_2 storage project. The reason is again the CEE, strongly affecting the average core saturation during the non-wetting phase monophasic injection (when f_w=0 during the SS-method). The low CO_2 viscosity can partially explain this difficulty. The lowest brine saturation measured during the coreflood experiments is referred as the residual water saturation (S_{wr}). Access to the local saturations using in-situ imaging techniques provides a convenient solution to narrow the gap between the S_{wr} and the S_{wir} values, providing the CEE doesn't extend beyond the core length. Still, flow simulations or history match is required to have a correct estimation of the k_r-values for these local saturations, when using either the SS- or the US-method.

When measuring the flow properties for the pair of fluids CO_2/brine, these difficulties encountered with these two methods are exacerbated. The low CO_2's viscosity at reservoir conditions causes lower pressure gradient in the CO_2 phase, and advert mobility ratio when injecting the CO_2. Consequently, the drainage is more disturbed by CEE, the front displacement is less stable, and the residual water saturation is less reachable. In addition, the lower CO_2 density causes gravitational segregation for horizontal cores.

The objectives of the work presented here is to reconciliate these two methods (the SS- and the US-method) and to get "best practices" when measuring k_r-curves with CO_2. K_r-curves have been measured for these fluids using the two protocols presented above, on a homogenous Grès-de-Fontainebleau sandstone. Experiments were conducted at reservoir conditions (54°C, 90bars), using the mini-coreflood injection platform CAL-X™ [32]. This set-up limits the plug size to a typical core length of 20mm but provides a qualitative access to the local saturations. A capillary pressure curve has also been measured using the SDM technique, to provide the P_c inputs for the US experiments interpretation, and a better estimation of the S_{wir} value.

2 Materials and methods

2.1 Fluids and sample properties

All experiments have been conducted on the same plug: a clean Grès-de-Fontainebleau with intermediate porosity (12.7%) and permeability. The main petrophysical properties of the plug are given in Table 1. The initial core permeability K has been measured to 304 md using increasing injection flow rates of brine water (non-equilibrated with CO_2). The permeability is re-assessed before each experiment by injecting the brine at a constant flow rate of 0.5 cc/min (254 ft/d). The evolution of this permeability (referred as Kw) during time is given in **Fig. 1**. It shows a first quick drawdown of the initial value, followed by a stabilization around K_w = 150 mD. When computing the k_r-curves, the K_w value measured before running the experiment is use.

Table 1. Core main petrophysical properties.

Rock	Grès-de-Fontainebleau
Type	Sandstone
Length, Diameter (L/D)	20.4 mm, 9.65 mm
Porosity, Permeability (ϕ/K)	12.7%, - 304 mD
Pore volume (PV)	0.189 cc

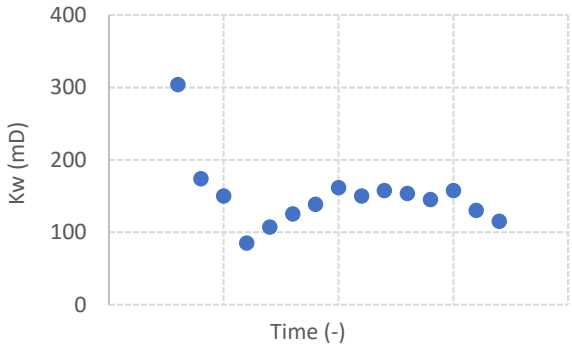

Fig. 1. Evolution of the plug absolute permeability during the study.

Supercritical CO_2 and a 30 g/L NaCl brine (S30) are used for all experiments. Properties of the fluids at the experimental conditions (54°C, 90bars) are given in **Table 2**. They show a viscosity ratio of μ_{CO2}/μ_{brine}= 0.04, leading to a strongly advert mobility ratio for CO_2 injection. Phases equilibriums are computed using modified Peng-Robinson equations [33].

One of the challenges when working with CO_2 and brine is the equilibration of each phase with respect to the other. While the two fluids are immiscible in our experimental conditions, a small fraction of each phase can be dissolved in the other one (mass transfer). This fraction is estimated to 1.6%mol of CO_2 dissolved in the brine, and 0.4%mol of brine dissolved in the CO_2 at 54°C and 90bar. If these fluids were injected with no prior equilibration, mass transfer will occur in the porous media leading to no phase trapping, and the measured k_r-curves will not be representative of in-depth reservoir flow.

The effect of injecting non-equilibrated fluids on the saturation endpoints can be easily estimated, assuming instantaneous and total phases equilibrium. During an imbibition, a residual CO_2 saturation Sr_{co2} of 40% can be entirely dissolved within less than 3 injected pore-volumes (PV) of unequilibrated brine. Similarly, during a drainage cycle, a residual water saturation S_{wr} of 20% can be entirely dissolved within 476 PV of unequilibrated CO_2. As already mentioned by [34, 35], the injection of unequilibrated fluids is less impacting when injecting CO_2 than when injecting the brine.

Table 2: Main fluids properties at experimental conditions.

	CO_2	30 g/L NaCl Brine
Conditions	54°C, 90 bars	
State	Supercritical	Liquid
Density (kg/m3)	260.5	1007.8
Viscosity (cP)	0.022	0.550
Molar composition when equilibrated	99.6% CO_2 0.4% Brine	98.4% Brine 1.6% CO_2

2.2 Experimental set-up and fluids equilibration system

Experiments have been conducted with the mini-coreflood injection platform CAL-X™. Technical aspects of this setup can be found in a previous work [32]. The fluids saturation is computed using interpretation of X-Ray radiographies taken every 10 seconds. As mentioned by [36], small cores are more subject to CEE than longer cores, but we intent to compensate this limitation by using high flowrates, access to the local saturations, and history matching techniques.

The effect of the temperature on the CO_2 solubility in the brine and the brine solubility in CO_2 is shown in **Fig. 3**. It shows an opposite behavior for the two fluids: the CO_2 solubility decreases with the temperature while the brine solubility increases with the temperature. The design of the fluids equilibration system takes advantage of this effect for the CO_2 solubility. A schematic view is given in **Fig. 2**. The two fluids are equilibrated at the experiment pressure and temperature conditions (T_{exp} and P_{exp}) in separated cells of 750 mL capacity. Equilibration is performed during a minimum duration of 12h. Once equilibrated, the two fluids are transferred in two ISCO pumps of 180mL capacity, at P_{exp} but ambient temperature (T_{amb} = 20°C). Finally, the ISCO pumps are used to inject or co-inject the equilibrated fluids in the core, at reservoir conditions (P_{exp} and T_{exp}).

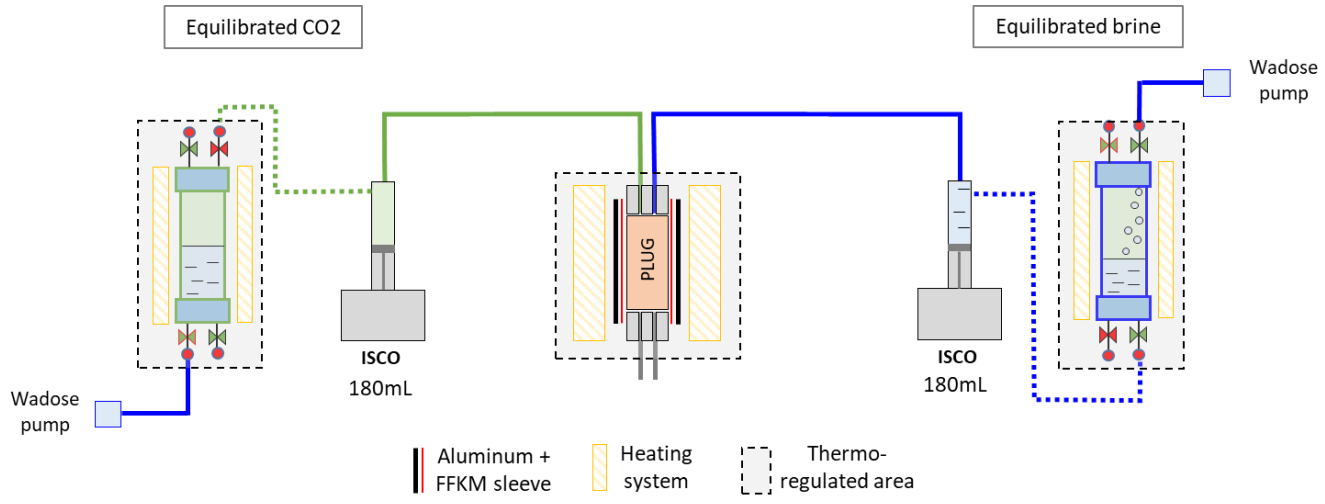

Fig. 2. Schematic view of the coreflooding setup and fluids equilibration system.

The experimental setup is not designed to have the equilibrated fluids kept at T_{exp} during the entire process (from equilibration to injection). Their storage at T_{amb} in the ISCO pumps is not a concern for the brine phase: the brine is under-equilibrated for temperature lower than T_{exp}, and no CO_2 exsolution should occur during this step. The situation for the CO_2 is different: the brine solubility at T_{amb} is 40% lower than at T_{exp}, leading to phases separation in the ISCO pumps. The injected CO_2 is therefore 40% under-equilibrated when injected in the core. However, this should not significantly impact the kr-curves measurements: it was stated above that the injection of unequilibrated CO_2 was only an issue if large number of PV were injected. Yet, minor effect of this under-equilibrium might be observed near the core inlet [29].

Temperature homogeneity and control during the experiments has been a real challenge during the experiments. The CAL-X™ setup uses a local temperature regulation system, wrapping the injection cell. Although the fluids are pre-heated in the injection lines, their injection at high flowrates can destabilize the core temperature homogeneity. Two PT100 temperature sensors are used to monitor the temperature during the experiments. The sensors are installed in the inlet and outlet injection heads.

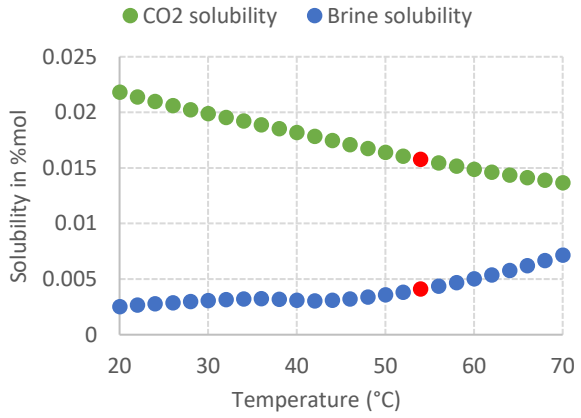

Fig. 3. Effect of the temperature on the CO_2 and brine solubilities, at 90 bars. The red markers show the experimental conditions (54°C) of this study.

2.3 Experimental procedure

This section gives details on how the two k_r and P_c curves have been interpreted using the SS, US and SDM methods, respectively. Only drainage experiments have been conducted (CO_2 displacing the brine), and the steady-state experiment has been performed using decreasing water fractional flow (f_w). They all started with the core initially saturated with the brine. Injection was conducted from top to bottom to mitigate gravitational effect when injecting the CO_2.

2.3.1 SS-method

The CO_2 and the brine were co-injected at increasing CO_2 fractional flow. The total volume flowrate was not kept constant during the experiment: it is increased by 4 from f_w = 100% to f_w = 0%, to compensate for the lower CO_2 viscosity. The k_r-values were interpreted using the simplified Darcy's equations for multiphases flow (**Eq. 1**) with the hypothesis of laminar flow and constant capillary pressure. Laminar condition is verified since a linear relation between flow rate and pressure drop is respected in mono-phasic injection. To verify for a constant capillary pressure, the saturation at steady state condition must be uniform along the sample. If these conditions are respected, we can consider an equal pressure drop in the wetting and non-wetting phases ($\Delta P_{brine} = \Delta P_{CO2}$) [38].

$$\begin{cases} k_{rw}(S_w) = \dfrac{\mu_w L}{K_w S} * \dfrac{Q_{brine}^{core}}{\Delta P_{brine}} \\ k_{rCO2}(S_w) = \dfrac{\mu_{CO2} L}{K_w S} * \dfrac{Q_{CO2}^{core}}{\Delta P_{CO2}} \end{cases} \qquad \textbf{Eq. 1}$$

2.3.2 US-method

Only CO_2 was injected during the US-method with the sample initially saturated with equilibrated brine. CO_2 was injected at a volume flowrate of 1.57 cc/min (800 ft/d), for a total of 800PV. It was circulated at the core inlet face prior to its injection in the core, to favor a best boundary injection condition. No increasing flowrates were used to avoid temperature variation. The X-ray frequency acquisition was increased by 5 (i.e., one radiography every 2s) to better resolve the transient state.

The estimation of the k_r-curves was performed through history match using the commercial solution CYDAR™. Before doing so, it is crucial to clearly identify the parameters that can be tuned during the fitting process:

1. The experimental data that will be used to constrain the history match, and the associated level of confidence. Here, these data were the average saturation (vs time) and the differential pressure (vs time). The saturation profiles were not integrated in the optimization process, but only one saturation profile (the last one) has been used for a quality check.
2. The input properties that should not be changed, such as the fluids properties (viscosity, density), the core properties (K, ϕ, dimensions) and the injection sequence (duration and flowrates).
3. The input properties that might be changed in a reasonable extension. Here, the P_c-curve measured during the SDM experiment was an input for the history match, but a small deviation from the experimental data has been allowed.
4. The output properties that should be fitted. Here, these properties were the k_r-curves, and they were initiated with the k_r-curves obtained through the SS-method.

History match is a powerful tool to estimate properties. Yet, if no care is taken during the process,

multiple "best-fits" can be obtained with very completely different fitted properties. Hence the prior analysis of the different input properties. The set of k_r-curves obtained through the SS-method was used to initiate this property during the history match. This limits the possibility of fitting the experimental data with misleading solutions.

The k_r-curves were described using the Corey's description (**Eq. 2**):

$$\begin{cases} k_{rw}(S_w) = k_{rw}^{max} * \left(\frac{S_w - S_{wi}}{1 - S_{wi}}\right)^{nw} \\ k_{rCO2}(S_w) = k_{rCO2}^{max} * \left(1 - \frac{S_w - S_{wi}}{1 - S_{wi}}\right)^{nCO2} \end{cases} \quad \textbf{Eq. 2}$$

2.3.3 SDM

The SDM was used to estimate the inlet P_c-curve for the drainage displacement (CO_2 injection). CO_2 was injected at increasing flowrates, from 0.15 cc/min (76 ft/d) to 1.57 cc/min (800 ft/d). The flowrates were increased once the differential pressure (dP) and the saturations stabilized. The P_c-values are directly given by the dP measured between the core inlet and outlet (**Eq. 3**). The relevant saturation in the SDM is the inlet saturation. The latter was estimated using the local saturations measured over the first 3 mm of the core (**Fig. 4**). The brine water was also circulated at the core outlet at 0.2 cc/min (102 ft/d). This allows to have the outlet pressure measured in the brine phase (P_{brine}^{outlet}), while the inlet pressure is measured in the CO_2 phase (P_{CO2}^{inlet}. As the brine is immobile in the sample, we can consider the inlet and outlet pressure to be equal in the brine phase ($P_{brine}^{outlet} = P_{brine}^{inlet}$). Doing so, the capillary pressure at the core inlet can be directly computed using **Eq. 3.**

$$P_c\left(1 - S_{CO_2}^{inlet}\right) = P_{CO_2}^{inlet} - P_{brine}^{oulet} = dP \quad \textbf{Eq. 3}$$

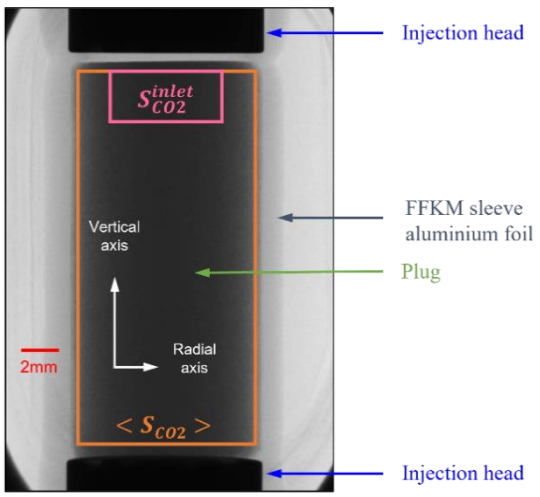

Fig. 4. X-ray radio-projection of the core and the cell, showing the spatial area for the average and the inlet saturations measurements, represented in orange and pink, respectively.

3 Results and discussion

For the three experiments, the monitoring included the fluids flowrates in cc/min (brine and CO_2), the inlet (top) and outlet (bottom) temperatures in °C, the differential pressure in mbars (dP), and the core saturation (S_{CO2}). For the SDM, the inlet saturation is also given.

3.1 SDM - P_c-curve

The P_c-curve was estimated using the SDM technique. **Fig. 5** shows all the time-series recorded during the experiments. The retained values for the P_c-curve estimation are given in **Table 3**.

Temperatures recorded during this experiment on the top of the sample corresponding to the inlet (cf. **Fig. 5)** showed strong dependency to CO_2 flow rate while the temperature at the bottom remain rather constant due to the brine sweeping. A gradient of 3°C was observed between the core inlet and outlet during the early steps of the drainage, and the inlet temperature was decreased by almost 3°C during the experiment. As the CO_2 was injected at ambient temperature (around 20°C), its injection in the core slightly cool down the core inlet. This is due to heat exchange between the injected fluid and the core holder, which is dependant of the flow rate. These two effects (temperature gradient and inlet temperature variations) are impacting several aspects of the experiment interpretation. Indeed, beside its effect on the fluid's equilibrium, it also affects the saturation quantification using the X-ray and the CO_2 viscosity.

Fig. 6 shows the P_c-curve computed for this experiment before and after corrections to account for the temperature variations (respectively the red and the blue dots). The dP have been corrected using the CO_2 viscosity variations, computed using the average core temperature. The inlet brine saturations have been corrected using the inlet temperature variations and a prior X-ray/temperature calibration experiment. After correction, the inlet S_{wr} value obtained during highest CO_2 flowrate is estimated to 16% (9% before correction), while the average core saturation is estimated to 20% (before correction). The interpreted P_c-values only cover a limited range of CO_2 saturations, with all values falling within 60 and 90 bars. The SDM does not allow to reach low CO_2 saturations, for the same reason as mentioned for the US-method in the introduction. It can also be supposed that higher CO_2 saturations could have been obtained using a higher injection flowrate, as the asymptotic section of the curve has not been reached. This portion of the P_c-curve is challenging to describe, precisely because of this asymptotic behavior at high CO_2 saturations.

The data were fitted using a 3-parameters $\log(S^{beta})$ function with no threshold (cf. CYDAR™ Pc-curve functions). The grey and black curves (**Fig. 6**) show the magnitude of uncertainty that was given to the experimental data considering the ad-hoc corrections that has been made on the dP and the saturations. The latter has been used as the Pc input during the history match of the US experiment. During the fitting process, the S_w value was given to 6%, while the lowest inlet saturation

observed during the experiment was S_{wr} = 16%. It shall be noted this S_w value was not set during the history match process; it was one of the fitting parameters. Only its range was constrained from 0% to 16%, and it was initiated at 6%.

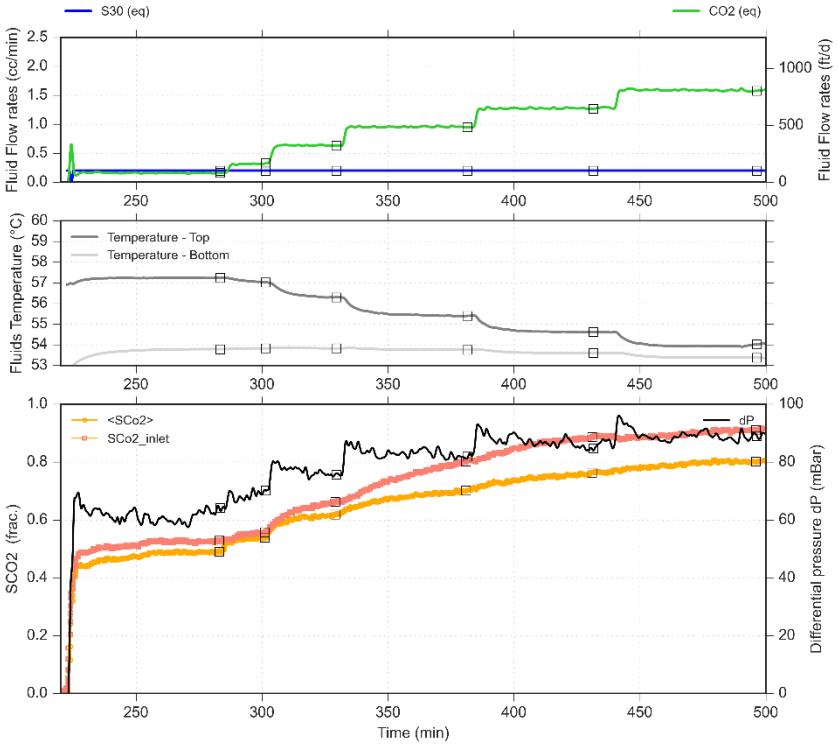

Fig. 5. Flowrates (S30 and CO_2), temperatures (inlet and outlet), saturations (inlet in pink, and average in orange) and differential pressures monitoring during the SDM. The square markers show the values retained for the P_c-curve estimation.

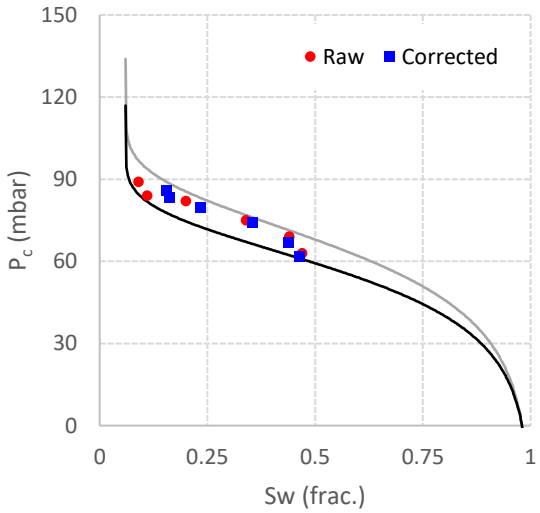

Fig. 6. Pc-curve obtained with the SDM experiment. The blue dots are obtained after dP and inlet S_w corrections. The grey and black curves show the analytical function used for the P_c-curve description, and the interval of confidence that was given to these data.

Table 3: Retained values for the Pc-curve estimation.

N°	Q_{CO2} (cc/min)	dP (mbar)	S_w (frac.) inlet	dP (mbar) corrected	S_w (frac.) inlet corrected
1	0.16	63	0.47	62	0.46
2	0.32	69	0.44	67	0.44
3	0.63	75	0.34	74	0.36
4	0.95	82	0.2	80	0.24
5	1.27	84	0.11	83	0.16
6	1.57	89	0.09	86	0.16

3.2 Kr-curves – SS-method

Measurements recorded during the SS-methods are given in **Fig. 7**. The values retained for the k_r-curves interpretation are given in Table 4. 2D saturations maps corresponding to some of these f_w steps are shown in **Fig. 8**, with the corresponding saturations profiles (**Fig. 9**)

The temperatures showed less variations during this experiment than previously observed during the SDM experiment. An average temperature decreased of 1°C was observed between the first and the last flowrates. This difference in the temperature behavior is mainly due to the difference in heat capacity, molar mass, and density of brine and CO_2 respectively.

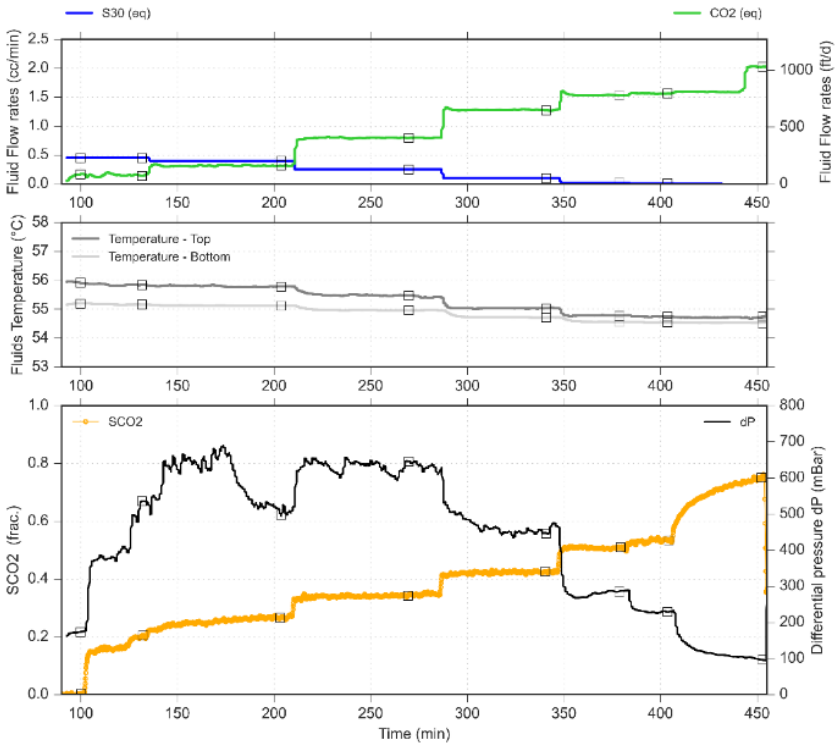

Fig. 7. Flowrates (S30 and CO_2), temperatures (inlet and outlet), average saturation (in orange) and differential pressure monitoring during the SS-method. The square markers show the values retained for the k_r-curve estimation.

The dP signal recorded for the first steps showed lack of stability of the two-phases flow displacement, until a critical CO_2 saturation is reached. The saturation maps for the step N°3 (**Fig. 8**) clearly showed a lack of saturation homogeneity all along the core. Those instabilities might be caused by the SS-method itself: the co-injection of the CO_2 and the brine at small CO_2 fractional flow imposes low CO_2 saturations. For these points, the CO_2 saturation was not high enough to reach its critical saturation at which it could percolate homogenously through the core. Consequently, the CO_2 phase was partitioned in the core. The lack of stable dP for low saturations has already been observed by [37, 38], and they explained it by a regime of ganglia traffic, where the injected phase is flowing as a disconnected phase. In this experiment, the dP signal seemed to stabilize for $S_{CO2} > 42\%$, corresponding to the step N°5, although the 2D saturation maps for this step (**Fig. 8**) still show some phases partitioning in the upper part of the core. Once this critical saturation was reached (steps N°6 to 8), the differential pressure was more stable, and the local saturations shows (**Fig. 8**) a homogenous distribution, with no CEE, except for step N°8 where only CO_2 was injected (**Fig. 9**, fw=0.0). This observation clearly shows that the simplified Darcy's equations (Eq. 1) no longer apply for the k_r-value estimation.

This data shows that a stable injection of CO_2 could not be reached until the water fractional flow f_w became lower than 10%. This is well explained by the fluids advert viscosity ratio, yet it shows the difficulty to construct the k_r-curves with the co-injection method. Even if low average CO_2 saturations have been reaching during the experiment (steps N° 2 to 4), they are not truly representative of the core saturation and their interpretation should be taken with caution. In these experimental conditions, the SS-method ends-up showing similar limitation than the US-method when it comes to describing the k_r-curves for CO_2 low saturations. The kr-curves itself becomes challenging to construct using only f_w lower than 10%.

During the experiment, the lower average brine saturation was measured to S_{wr} = 24% at the end of the monophasic CO_2 injection. As mentioned above, this step is strongly impacted by CEE, and a lower brine saturation could be estimated between 15% and 20% using the 2D the saturation maps at the core inlet.

The k_r-curves obtained with the SS-method using **Eq. 1** are given in **Fig. 13** (square markers). It is discussed and compared with the curves obtained with the US-method in section 3.3.

Table 4: Flow rates, f_w, S_{CO2} and dP retained for SS-method.

N°	Q_{CO2} (cc/min)	Q_w (cc/min)	f_w (frac.)	dP (mbar)	S_{CO2} (frac.)
1	0.00	0.50	1.00	150	0.00
2	0.15	0.45	0.75	533	0.20
3	0.32	0.40	0.56	509	0.27
4	0.80	0.25	0.24	644	0.34
5	1.27	0.10	0.07	446	0.42
6	1.53	0.02	0.013	286	0.51
7	1.56	0.01	0.006	230	0.53
8	2.03	0.00	0.00	96	0.76

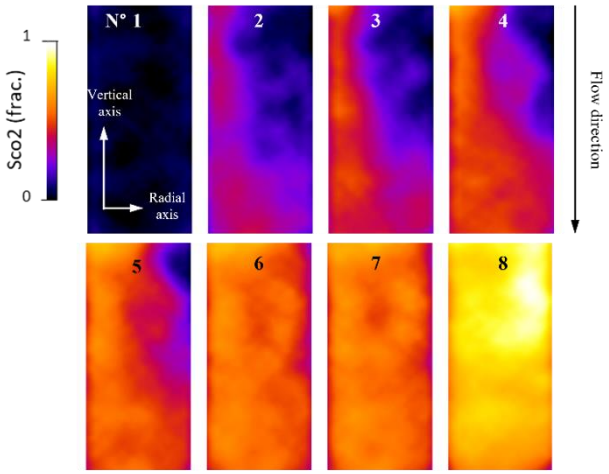

Fig. 8. 2D CO_2 saturation maps, taken at the end of the different steps of the SS-methods.

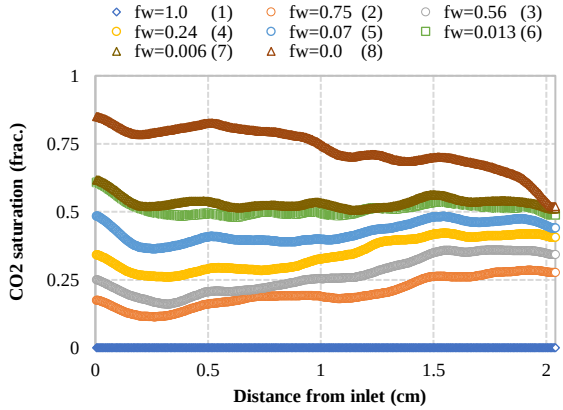

Fig. 9. CO_2 saturations profiles, taken at the end of the different steps of the SS-method.

3.2 Kr-curves – US-method

Measurements recorded during the US-methods are given in **Fig. 11**. 2D saturations maps taken at increasing step times during the early times of the displacement are shown in **Fig. 10**. The front of displacement shows a stable front displacement considering the CO_2 viscosity. This is mainly due to the core small size, mitigating the instabilities to occur at more than the millimeter scale. The temperatures (**Fig. 11**) show limited variations (around 1°C) compared to the SDM, as the CO_2 was injected at a constant flow rate and no brine was circulated at the core outlet.

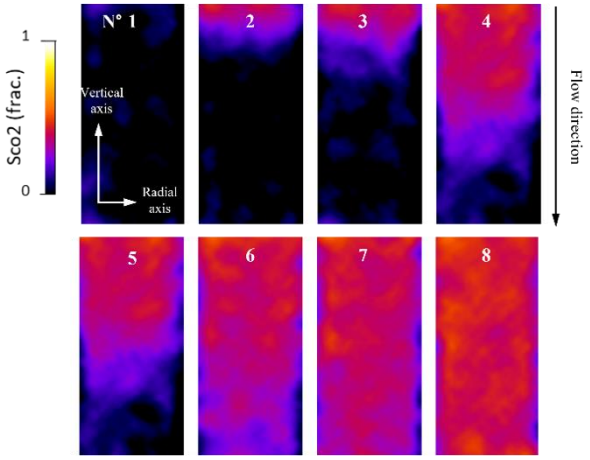

Fig. 10. 2D CO_2 saturation maps, taken at increasing steps of the US-methods.

As mentioned above, the dP and the average core saturation are used to constraint the history match. The P_c-curve obtained during the SDM is used as an input with a small deviation allowed. A saturation profile taken at the end of the experiment was also used to quality check to CEE and the P_c input. Results of the history match are shown in **Fig. 12**, with the markers showing the experimental data and the plain lines showing the simulated results.

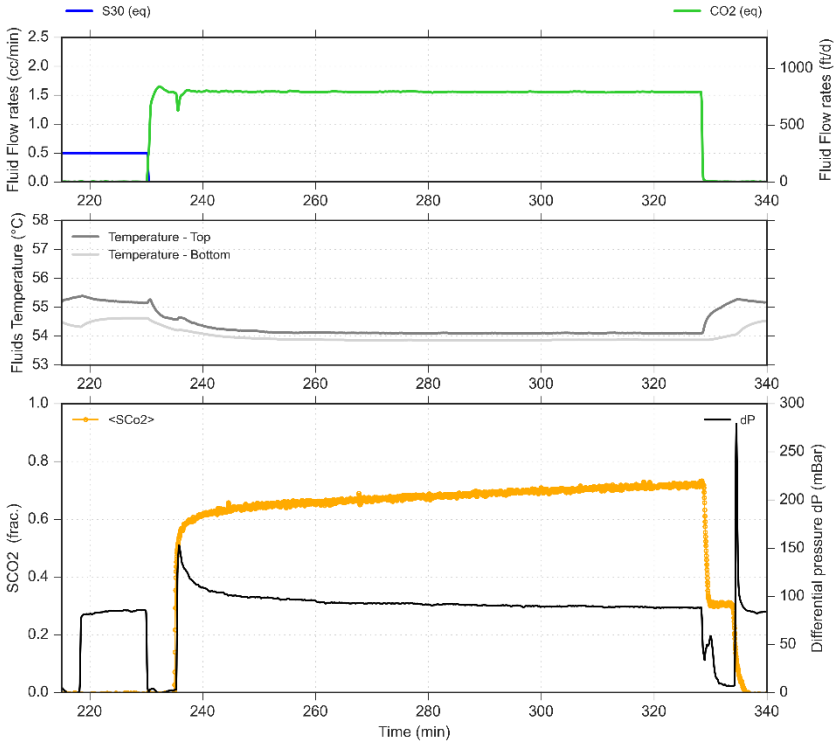

Fig. 11. Flowrates (S30 and CO_2), temperatures (inlet and outlet), average saturation (in orange) and differential pressure monitoring during the US-method.

The simulated average saturations and dP demonstrate an excellent match. The saturation profile shows a satisfactory match, validating the P_c-input. This quality check is crucial as an inconsistent P_c-curve will lead to an erroneous k_r-curves estimation. The major discrepancy between the data and the simulated saturation profile is the saturation at the core outlet. The simulated saturation profile shows a null CO_2 saturation at the core outlet, imposed by the boundary condition $P_c = 0$, while the experimental data suggests a CO_2 saturation > 25%. While some errors regarding the saturation estimation might occur near the core boundaries, the null saturation at the outlet is more a numerical artefact than a reality. As the CO_2 is injected at a constant flow rate, it has to flow-out of the sample, and thus CO_2 saturation cannot be null even at the core outlet.

The final average brine saturation is measured to S_{wr} = 27%, and the inlet saturation to 15%. These values are in-line with the previous estimations obtained with the SS-method and during the SDM. Still, the saturation profile suggests that the CEE might extend beyond the core length in these injection conditions. And therefore, that the S_{wr} = 15% measured at the core inlet is only an overestimation of the S_{wir} value.

The k_r-curves obtained with the US-method are given in **Fig. 13** (plain curves). It is discussed and compared with the curves obtained with the SS-method in section 3.3.

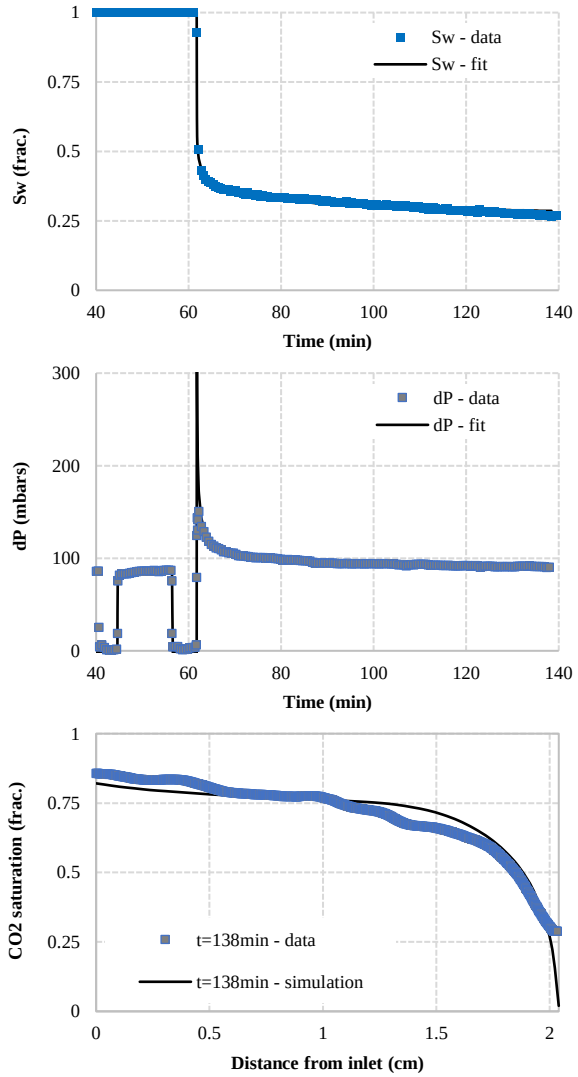

Fig. 12. History match of the US-drainage experiment. The S_w and dP measurements have been used for the optimization while the saturation profile taken at the end of the experiment (t=138min) is used for quality check only.

3.3 Kr-curves – Comparison and discussion

Fig. 13 shows the CO_2 (in green) and the brine (in blue) k_r-curves obtained with the SS-method (analytical solution) and with the US-method (history match). The two methods show an excellent comparison, except for the point marked by the black arrow in **Fig. 13**. This point corresponds to the last step of the SS-method, where only CO_2 was injected. The k_r-value has been estimated using the simplified Darcy's equations that no longer apply when the CEE prevails. The SS-method was expected to provide a poor estimation of this point, with both an underestimation of the k_r-value and an overestimation of the lower brine saturation. The simulation performed using CYDAR™ account for these capillary-end effects, and therefore provides a more reliable estimation of the k_r-curves for low brine saturations.

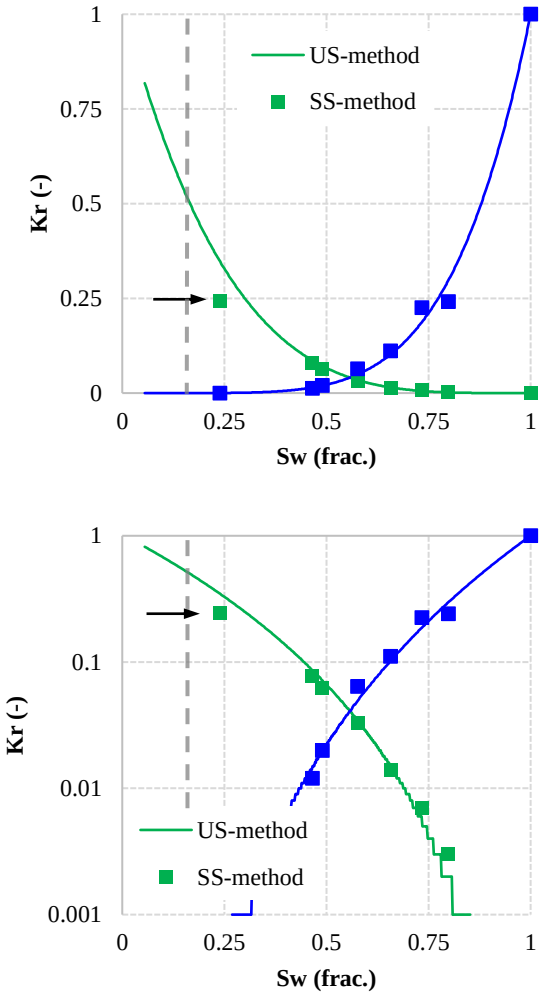

Fig. 13 : Comparison of the k_r-curves obtained with the SS-method (analytical solution, Eq. 1) and with the US-method (history match, **Fig. 12**). The CO_2 kr-curves are shown in green; the brine kr-curves are shown in blue. The dash line indicates the lower local saturations estimated at the core inlet during the monophasic CO_2 injections. The values before this limit have been obtained during the history match process.

The grey dashed vertical line in **Fig. 13** shows the lowest brine saturations estimated at the core inlet during the monophasic injections. The later was estimated between 15% and 16% during the different experiments. Still the saturations profiles measured during the US-method (see **Fig. 12**) and the P_c-values estimated during the SDM suggested that the S_{wir} was probably lower than these estimations. A S_{wir} value of 5.5% have been obtained during the history match process, while no simulated local saturations went lower than 18%. And no satisfactory match could be obtained when constraining the history match with a higher S_{wir} values. The explanation might be found in the very slow decrease of the brine saturations during the late stages of the US-method. The brine become less and less mobile as its saturation decreases. Technically, the S_{wir} value can only be reached with an infinite injection of CO_2 (infinite at laboratory scale), allowing for the brine to be produced with extremely low kr-values ($< 10^{-3}$). It is therefore not surprising to obtain an estimation of the S_{wir} value (during

the history match) lower than the minimum saturation reached within the 80 minutes of CO_2 injection of this experiment. The numerical S_{wi} estimation is partially constraint by the experimental data of the brine mobility at slightly higher brine saturation (between 15% and 20%). In these conditions, the history match allows to complete the k_r-curve over the saturations ranges that could not been reached during the coreflood experiments.

The process of history matching has been repeated with no prior knowledge of the k_r-values provided by the SS-method. The k_r-curves were initiated with a random set of curves. Completely different solutions were obtained for the k_r-curves during the process. It shows that although it is a powerful tool, it can lead to misleading results if not contained correctly. For the context of this study, it shows the great advantage of combining the SS- and the US-method for the kr-curves estimation.

4 Conclusions

The purpose of this study was (1) to reconciliate the SS- and the US-methods in the context of k_r-curves measurement for CO_2 and brine at reservoir conditions (54°C, 90 bars); and (2) to find "best practices" when running these experiments. CO_2/brines k_r-curves are challenging to measure at reservoir conditions because of the high density and viscosity contrast between the CO_2 and the brine. These latter lead to a poor mobility control when injecting the CO_2, and the prevailing of CEE. These two effects tackle the limit of the SS- and the US-method. The combination of the two methods was found to provide meaningful information for the k_r-curves interpretation.

The SS-method was said to provide the most reliable k_r-curves, especially when advert mobility ratio is involved. We found that the construction of the curves was more difficult with this method. Even if it allows reaching lower CO_2 saturation than the US-method, the 2D saturations maps demonstrated that the saturation is highly heterogenous in the core, and the fluids flow is not stable as a regime of ganglia traffic might occur. These two observations are not compatible with the assumptions made when using the simplified analytical solution (see **Eq. 2**) to compute the k_r-values. The suitable conditions to apply the analytical solution (homogenous saturation, stable flow regime) was only found for $f_w < 10\%$, limiting the number of experimental data points to construct the k_r-curves. Finally, as expected, the last point of the experiment ($f_w = 0\%$) was found to be strongly affected by the CEE, and to provide an erroneous estimation of the k_r-value.

The US-method was found to be a powerful tool to interpret the data of the unsteady-state displacement. It is especially true when coupled with both the SDM and the SS-experiments to provide relevant P_c-curves and k_r-curves inputs. A prior approximate knowledge of the k_r-curves has demonstrated being critical to initiate the properties that were fitted during the history match. Access to the local saturations was also a key element in this work, giving the possibility to quality-check the simulated CEE with experimental data. A better confidence in the input P_c-curve leads to a higher confidence in the kr-curves outcome.

The estimation of the S_{wi} value remains challenging using coreflooding experiments. The use of high injection flowrates and access to the local saturation have contributed to measure brine saturation down to 15% at the core inlet. But additional observations (values of the P_c-curves and the end-effect saturation profile) have suggested that it was still an overestimation of the 'true' S_{wi} value. The history match process has compensated for the experimental limitations, allowing the description of k_r-curves for saturations lower than the ones observed during the experiments.

"Best practices" retained from this study to measure kr-curves for brine and CO_2 at reservoir conditions would be a combination of both the SS-method and the US-method. An independent measurement of the P_c-curve, used as an input for the history match, is also recommended to narrow the fitting process to the k_r-curves only. Finally, high injection flowrates and access to the local saturations have proven effective to improve the quality of the experimental data interpretation.

References

[1] Global warming of 1.5 C, 2018. [Online]. Available: https://www.researchgate.net/profile/peter-marcotullio/publication/330090901_sustainable_development_poverty_eradication_and_reducing_inequalities_in_global_warming_of_15c_an_ipcc_special_report/links/6386062b48124c2bc68128da/sustainable-development-poverty-eradication-and-reducing-inequalities-in-global-warming-of-15c-an-ipcc-special-report.pdf

[2] P. Kelemen, S. M. Benson, H. Pilorgé, P. Psarras, and J. Wilcox, "An Overview of the Status and Challenges of CO2 Storage in Minerals and Geological Formations," *Front. Clim.*, vol. 1, 2019, doi: 10.3389/fclim.2019.00009.

[3] *The emissions gap report 2017: A UN environment synthesis report*, 2017.

[4] National Academies Press (US), *Negative emissions technologies and reliable sequestration: A research agenda*. Washington DC: The National Academies Press, 2019.

[5] H. de Coninck and S. Benson, "Carbon Dioxide Capture and Storage: Issues and Prospects," *Annual Review of Environment and Resources*, vol. 39, pp. 243–270, 2014, doi: 10.1146/annurev-environ-032112-095222.

[6] A. Chadwick, R. Arts, O. Eiken, P. Williamson, and G. Williams, "Geophysical monitoring of the CO2 plume at Sleipner, North Sea - An outline review," in 2006, 303-+.

[7] C. Doughty and K. Pruess, "Modeling Supercritical Carbon Dioxide Injection in Heterogeneous Porous Media," *Vadose Zone Journal*, vol. 3, no. 3, pp. 837–847, 2004, doi: 10.2113/3.3.837.

[8] M. Flett, R. Gurton, and I. Taggart, "The Function of Gas-Water Relative Permeability Hysteresis in the Sequestration of Carbon Dioxide in Saline Formations," in 2004, SPE-88485-MS. Accessed: 4/17/2023.

[9] A. Kopp, H. Class, and R. Helmig, "Investigations on CO2 storage capacity in saline aquifers: Part 1. Dimensional analysis of flow processes and reservoir characteristics," *International Journal of Greenhouse Gas Control*, vol. 3, no. 3, pp. 263–276, 2009, doi: 10.1016/j.ijggc.2008.10.002.

[10] R. Juanes, E. J. Spiteri, F. M. Orr, and M. J. Blunt, "Impact of relative permeability hysteresis on geological CO 2 storage," *Water Resour. Res.*, vol. 42, no. 12, 2006, doi: 10.1029/2005WR004806.

[11] A. Kumar *et al.*, "Reservoir Simulation of CO2 Storage in Deep Saline Aquifers," *SPE J.*, vol. 10, no. 03, pp. 336–348, 2005, doi: 10.2118/89343-PA.

[12] E. J. Spiteri and R. Juanes, "Impact of relative permeability hysteresis on the numerical simulation of WAG injection," *Journal of Petroleum Science and Engineering*, vol. 50, no. 2, pp. 115–139, 2006, doi: 10.1016/j.petrol.2005.09.004.

[13] M. Burton, N. Kumar, and S. L. Bryant, "CO2 injectivity into brine aquifers: Why relative permeability matters as much as absolute permeability," *Energy Procedia*, vol. 1, no. 1, pp. 3091–3098, 2009, doi: 10.1016/j.egypro.2009.02.089.

[14] *Relative permeability for multi-phase flow in CO2 storage reservoirs. Part II: resolving fundamental issues and filling data gaps*, 2015. [Online]. Available: https://scholar.google.com/citations?user=r8ghdzoaaaaj&hl=fr&oi=sra

[15] R. Lenormand, A. Eisenzimmer, and C. Zarcone, "A novel method for the determination of water/oil capillary pressures of mixed wettability samples," *SCA Conference Paper*, 1993, 1993. http://jgmaas.com/SCA/1993/SCA1993-22.pdf

[16] T. S. Ramakrishnan and A. Cappiello, "A new technique to measure static and dynamic properties of a partially saturated porous medium," *Chemical Engineering Science*, vol. 46, no. 4, pp. 1157–1163, 1991, doi: 10.1016/0009-2509(91)85109-B.

[17] R. Lenormand, A. Eisenzimmer, and P. Delaplace, "Improvements of the Semi-Dynamic method for capillary pressure measurements," *SCA Conference Paper*, 1995, 1995. http://www.jgmaas.com/SCA/1995/SCA1995-31.pdf

[18] M. Honarpour and S. M. Mahmood, "Relative-Permeability Measurements: An Overview," *Journal of Petroleum Technology*, vol. 40, no. 08, pp. 963–966, 1988, doi: 10.2118/18565-PA.

[19] Maini, "A Comparison Of Steady-State And Unsteady-State Relative Permeabilities Of Viscous Oil And Water In Ottawa Sand," *J Can Pet Technol*, vol. 29, no. 2, 1990.

[20] O. O. Eleri, A. Graue, and A. Skauge, "Steady-State and Unsteady-State Two-Phase Relative Permeability Hysteresis and Measurements of Three-Phase Relative Permeabilities Using Imaging Techniques," in 1995.

[21] R. Gupta and D. R. Maloney, "Intercept Method—A Novel Technique To Correct Steady-State Relative Permeability Data for Capillary End Effects," *SPE Reservoir Evaluation & Engineering*, vol. 19, no. 02, pp. 316–330, 2016, doi: 10.2118/171797-PA.

[22] Leverett, "Capillary Behavior in Porous Solids," *Trans. AIME*, vol. 142, no. 1, p. 152, 1941.

[23] Osoba, "Laboratory Measurements of Relative Permeability," *J Pet Technol*, vol. 3, no. 2, p. 47, 1951.

[24] S. E. Buckley and M. C. Leverett, "Mechanism of Fluid Displacement in Sands," *Transactions of the AIME*, vol. 146, no. 01, pp. 107–116, 1942, doi: 10.2118/942107-G.

[25] Richardson, "The Calculation of Waterflood Recovery From Steady-State Relative Permeability Data," *J Pet Technol*, vol. 9, no. 5, p. 64, 1957.

[26] Rapoport, "Properties of Linear Waterfloods," *J Pet Technol*, vol. 5, no. 5, p. 139, 1953.

[27] Kyte, "Linear Waterflood Behavior and End Effects in Water-Wet Porous Media," *J Pet Technol*, vol. 10, no. 10, p. 47, 1958.

[28] E. M. Braun and R. J. Blackwell, "A Steady-State Technique for Measuring Oil-Water Relative Permeability Curves at Reservoir Conditions," in *SPE Annual Technical Conference and Exhibition*, San Antonio, Texas, 1981.

[29] S. Berg, S. Oedai, and H. Ott, "Displacement and mass transfer between saturated and unsaturated CO2–brine systems in sandstone," *International Journal of Greenhouse Gas Control*, vol. 12, pp. 478–492, 2013, doi: 10.1016/j.ijggc.2011.04.005.

[30] S. C. M. Krevor, R. Pini, L. Zuo, and S. M. Benson, "Relative permeability and trapping of CO 2 and water in sandstone rocks at reservoir conditions," *Water Resour. Res.*, vol. 48, no. 2, 2012, doi: 10.1029/2011WR010859.

[31] J. Kokkedee, W. Boom, A. Frens, and J. Maas, "Improved Special Core Analysis: Scope for a reduced residual oil saturation," *SCA Conference Paper*, 1996, 1996. http://www.jgmaas.com/SCA/1996/SCA1996-01.pdf

[32] S. Youssef, M. Mascle, and O. Vizika, "High Throughput Coreflood Experimentation as a Tool for EOR Project Design," in *Day 4 Tue, April 17, 2018*, Tulsa, Oklahoma, USA, 04142018.

[33] I. Søreide and C. H. Whitson, "Peng-Robinson predictions for hydrocarbons, CO2, N2, and H2 S with pure water and NaCI brine," *Fluid Phase Equilibria*, vol. 77, pp. 217–240, 1992, doi: 10.1016/0378-3812(92)85105-H.

[34] W. Yan and E. H. Stenby, "The Influence of CO2 Solubility in Brine on CO2 Flooding Simulation," *SPE Annual Technical Conference and Exhibition*, 2009, doi: 10.2118/124628-MS.

[35] Ott, "Rock/fluid interaction by injection of supercritical CO2/H2S: investigation of dry-zone formation near the injection well," p. 1, 2010.

[36] R. E. Hinkley and L. A. Davis, “Capillary Pressure Discontinuities and End Effects in Homogeneous Composite Cores: Effect of Flow Rate and Wettability,” in 1986.

[37] D. G. Avraam and A. C. Payatakes, “Flow regimes and relative permeabilities during steady-state two-phase flow in porous media,” *Journal of Fluid Mechanics*, vol. 293, pp. 207–236, 1995, doi: 10.1017/S0022112095001698.

[38] C. D. Tsakiroglou, D. G. Avraam, and A. C. Payatakes, “Transient and steady-state relative permeabilities from two-phase flow experiments in planar pore networks,” *Advances in Water Resources*, vol. 30, no. 9, pp. 1981–1992, 2007, doi: 10.1016/j.advwatres.2007.04.002.